Available online at www.sciencedirect.com
ScienceDirect
International Journal of Multiphase Flow 32 (2006) 1300–1310
International Journal of Multiphase Flow
www.elsevier.com/locate/ijmulflow

Brief communication

Flow boiling of organic binary mixtures

A. Levy *, A. Koyfman, M. Jelinek

Pearlstone Center for Aeronautical Engineering Studies, Mechanical Engineering Department, Ben-Gurion University of the Negev, P.O. Box 653, Beer-Sheva 84105, Israel

Received 19 July 2005; received in revised form 19 June 2006

Keywords: Flow boiling; Organic mixtures; Two-fluid model; Mixtures boiling

1. Introduction

Over the past few decades, the trend to replace the working fluid in refrigeration units with mixtures of refrigerants has motivated vast amounts of research on the transport properties of the new proposed working fluids (e.g., Inoue et al., 2002; Kattan et al., 1998a,b,c; Mishra et al., 1981; Ross et al., 1987). These studies aimed at finding the heat transfer coefficients of refrigerant mixtures with a low temperature glide during processes such as evaporation and condensation. A variety of experimental systems have been used to obtain heat transfer coefficients for convective flow boiling in horizontal tubes (Jung et al., 1989; Kattan et al., 1998b; Mishra et al., 1981; Ross et al., 1987; Sami et al., 1994; Wettermann and Steiner, 2000; Wojtan and Thome, 2003) and in vertical tubes (Barbosa and Hewitt, 2001a,b; Bennet and Chen, 1980; Rivera and Best, 1999; Steiner and Taborek, 1992; Toral et al., 1982). During evaporation, the heat transfer coefficients of solutions may be substantially smaller than those of the pure components of the mixtures. Experimental studies have shown that as the composition of the liquid and the vapour mixtures differs, the heat transfer coefficients decreases (Baehr and Stephan, 1998; Happle and Stephan, 1974; Inoue et al., 2002; Mishra et al., 1981). For a mixture with an azeotropic point, the difference between the molar concentrations of the components in the gas and the liquid phases becomes smaller as the azeotropic point is approached, and therefore the heat transfer coefficient increases.

In two-phase flow, different flow regimes give rise to different heat transfer coefficients (Steiner and Taborek, 1992). These heat transfer coefficients are also dependent on the mass flow rate of the phases, the vapour quality and the pipe geometry. For a mixture of miscible fluids (i.e., a solution), as is the case in this study, the heat transfer coefficients will also depend on the concentration of the volatile phase (which, in turn, depends on pressure and temperature) in both the liquid and the gaseous phases. A variety of methods have been proposed for calculating the heat transfer coefficients for various modes of flow (flow patterns) and heat transfer regions (Collier and Thome, 1994; Stephan, 1992; Thome, 1996).

* Corresponding author. Tel.: +972 7 6477092; fax: +972 7 6472813.
E-mail address: avi@bgu.ac.il (A. Levy).

0301-9322/$ - see front matter
doi:10.1016/j.ijmultiphaseflow.2006.06.007

Various theoretical approaches based on mass, momentum and energy balances have been used for modelling and numerical simulation of boiling flows. Among the models that take into consideration interactions between the phases and modes of flow in evaporation, condensation, absorption and desalination processes, the two-fluid model seems to be the most suitable approach for describing two-phase flow with heat and mass transfer (Prashanth and Seetharamu, 1993; Richter, 1983; Sujatha et al., 1997a,b; Yang and Zhang, 2005). There is, however, still the need to develop a reliable model for predicting flow characteristics along a vertical tube to facilitate further analysis of the system and to provide some of the design parameters for such a boiler.

In the present study, an experimental and numerical investigation of convective boiling of a binary organic solution, with a large temperature glide (above 200 °C), in a vertical tube was conducted. A continuous experimental system was designed, built and operated. The two-fluid model was used to model and simulate the flow and to obtain the characteristics of the flow profile along the vertical tube.

2. Experimental setup and results

The flow boiling of an organic mixture, composed of an organic solvent, dimethylacetamide (DMAC), and a hydrofluorocarbon refrigerant, chlorodifluorometane (R22), was investigated. The thermo-physical properties of the pure components are presented in Table 1. A schematic illustration of the flow boiling experimental system is presented in Fig. 1. The rich solution is pumped out of the reservoir, cools down and flows through the flowmeter to the heating unit (generator), where it gains heat and starts the boiling flow process. The desorption process in the generator creates small vapour bubbles, which subsequently merge into larger bubbles. The rising bubbles form slugs that occupy the whole cross-section of the glass tube and flow with the poor solution to the separating vessel. From the separating vessel, the gaseous phase flows up to the gas heat exchanger, and the poor solution flows to the solution heat exchanger. The cooled (but not condensed) refrigerant vapour and the poor solution enter the absorber, where the absorption process then takes place. The rich solution from the absorber flows back into the reservoir.

In our experimental set-up, the inside diameters of both the heating unit and the convective tube (including the glass section) were 7 mm. The 10-cm heating section was located 15 cm from the vertical tube inlet. The total length of the vertical tube, including the heating and the convective sections, was 1.23 m. Copper tubes (3/8 in.) bent into oval spirals served as the absorber, poor solution and refrigerant heat exchangers. *T* type (copper-constantan) thermocouples, with an accuracy of ±0.3 °C, were placed at various locations in the experimental system, but not in the generator or the convective tube (so as not to influence the flow characteristics). An STS pressure transducer [ATM model – measuring range of 0–20 bars; accurac ±0.1% of full scale (FS)] was used to measure the absolute system pressure. The volumetric flow rates of the poor and rich solutions were measured with Kobold Pelton turbine flowmeters (LM model, measuring range 0.02–1.3 ml/min; accuracy ±0.5% FS). The pressure drops across the convective tube and the generator were measured with a Smart differential pressure transducer (LD 301 model, calibrated to 0–200 mbar range; accuracy ±0.075% FS). Power, supplied to three 220 V/100 W electric heaters via a variable transformer (0–220 V), was measured with a digital wattmeter (accuracy ±1 W). Data from the sensors were recorded on a personal computer via a National Instruments DAQPad-4350 data logging system. The data logging application was written using National Instruments LabVIEW.

Table 1
Thermo-physical properties of the pure components of the solution

	DMAC	R22
Formula	$CH_3CON(CH_3)_2$	$CHClF_2$
M_w	87.12	86.47
T_b (°C)	165	−40.8
T_c (°C)	382.6	96.0
P_c (bar)	41.7	49.77

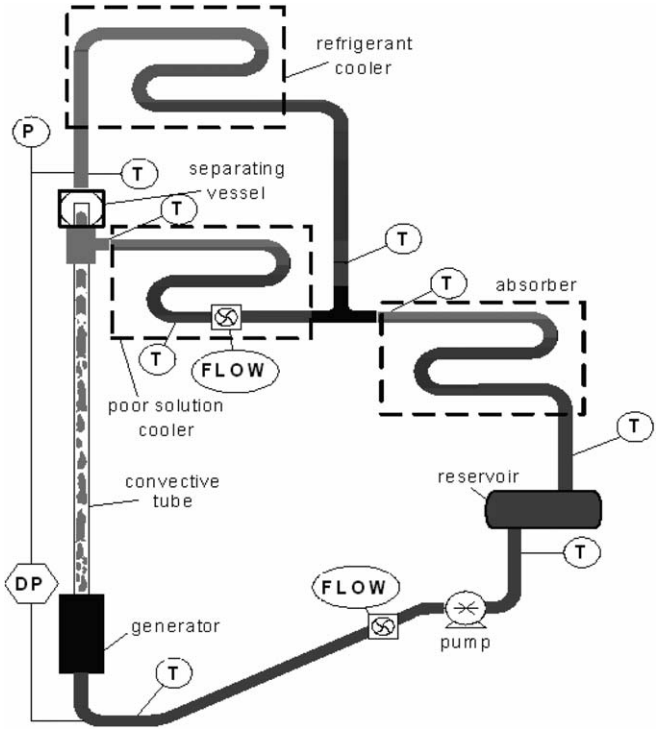

Fig. 1. Schematic illustration of the experimental system for flow boiling of organic solutions in a vertical tube.

Table 2
Time-averaged flow properties as obtained experimentally for various heat inputs

Heat supplied (W)	Temperatures (°C)								System pressure (10^{-5} Pa)	Pressure difference (10^{-2} Pa)	Rich solution flow rate (ml/min)	Poor solution flow rate (ml/min)
	Vertical tube inlet	Rfrigerant heat exchanger		Poor solution heat exchanger		Absorber heat exchanger		Reservoir outlet				
		Outlet	Inlet	Outlet	Inlet	Outlet	Inlet					
60	26.32	24.65	25.89	30.81	33.54	30.13	30.32	30.27	2.944	63.983	98.10	90.18
80	25.73	23.75	25.65	31.67	34.91	30.77	31.18	30.89	3.048	62.704	105.18	95.94
100	25.36	23.75	27.43	31.12	36.95	31.85	31.95	31.71	3.153	58.670	103.86	96.84
120	26.81	25.60	29.18	33.27	38.99	33.97	33.29	33.74	3.385	54.650	109.56	97.20
140	26.18	23.47	29.05	36.14	40.86	34.51	34.04	34.55	3.510	48.138	111.72	98.70
160	31.22	29.75	36.14	42.82	48.24	41.29	40.28	40.62	4.179	53.974	112.68	98.40
180	26.60	23.95	31.62	38.17	44.51	36.26	35.62	36.22	3.756	48.143	114.96	99.72
200	29.71	26.35	35.17	42.69	50.41	40.80	40.00	40.74	4.266	51.214	117.48	99.48
220	28.84	27.43	36.91	42.37	49.99	40.27	39.24	39.59	4.211	50.629	115.20	94.56

The laboratory system was operated continuously until steady state conditions were reached. Time-averaged flow properties recorded for various heat inputs under steady-state operating conditions are presented in Table 2.

3. Flow boiling model

Since the sub-cooled solution is inserted into the boiler located at the bottom of the vertical tube, the model should account for both single- and two-phase flows. Mass, momentum and energy balance equations were written for both types of flow. The conservation equations for the flow of a solution with a constant concentration of the refrigerant were solved for the single-phase flow. In the heating section, heat is supplied to the

solution until it reaches equilibrium conditions, i.e., until the equilibrium concentration of the refrigerant at the solution pressure and temperature is equal to that of the sub-cooled solution. When equilibrium is reached, the refrigerant starts to dissolve out of the solution due to additional heat transfer and pressure reduction; the concentration of the refrigerant in the solution decreases; two-phase flow is initiated and the volume fraction of the gas phase increases. Thus, conservation equations for the two-phase flow were solved. Generally, under equilibrium conditions, the gas phase is composed of both absorbent and refrigerant vapours. However, due to the large differences between the normal boiling temperatures of the absorbent and the refrigerant in our system (Table 1), i.e., the large temperature glide, the presence of absorbent vapour in the gas phase may be neglected, on condition that the solution temperature remains sufficiently below the saturation temperature of the absorbent.

In our model the following assumptions were made: one-dimensional flow; steady state flow; constant heat flux in the generator; constant tube diameter, i.e., cross-section area; uniform cross-section fluids properties; compressible gas and liquid phases; thermal equilibrium (i.e., both phases at the same temperature); absorbent vapour in the gas phase neglected; and friction force between the vapour phase and the wall neglected.

3.1. Single-phase flow governing equations ($\xi^* > \xi$)

Solution mass balance

$$\frac{\partial}{\partial z}(\rho_l u_l) = 0 \tag{1}$$

Solution momentum balance

$$\frac{\partial}{\partial z}(\rho_l u_l^2) + \frac{\partial P}{\partial z} = -F_{WL} - \rho_l g \tag{2}$$

Solution energy balance

$$\frac{\partial}{\partial z}\left(\rho_l u_l\left(h_l + \frac{u_l^2}{2}\right)\right) = \dot{q} \tag{3}$$

The enthalpy of the solution, h_l, was calculated as a function of the composition, ξ, the enthalpy of the refrigerant in the liquid hase, $h_{rl} = f(T)$, the enthalpy of the absorbent, $h_a = f(T)$ and the excess enthalpy of the solution, $\Delta h_{mix} = f(T, \xi)$ (Borde and Jelinek, 1986)

$$h_l = \xi h_{rl} + (1 - \xi)h_a + \Delta h_{mix} \tag{4}$$

The density of the solution was calculated as function of the composition and of the densities of the refrigerant and absorbent

$$\rho_l = \frac{1}{\xi/\rho_{rl} + (1 - \xi)/\rho_a} \tag{5}$$

The density of the absorbent was expressed as a function of the solution temperature, $\rho_a = f(T)$, while the density of the refrigerant in the liquid phase was expressed as a function of the solution pressure, i.e., $\rho_{rl} = f(P)$ (Jelinek et al., submitted for publication).

3.2. Two-phase flow governing equations

Total mass balance

$$\frac{\partial}{\partial z}((1 - \varphi)\rho_l u_l + \varphi\rho_g u_g) = 0 \tag{6}$$

Vapour phase mass balance

$$\frac{\partial}{\partial z}(\varphi\rho_g u_g) = \dot{m} \tag{7}$$

Refrigerant mass balance

$$\frac{\partial}{\partial z}((1-\varphi)\xi\rho_l u_l + \varphi\rho_g u_g) = 0 \tag{8}$$

Vapour phase momentum balance

$$\frac{\partial}{\partial z}(\varphi\rho_g u_g^2) + \varphi\frac{\partial P}{\partial z} = \dot{m}u_i - F_{gl} - \varphi\rho_g g \tag{9}$$

Total momentum balance

$$\frac{\partial}{\partial z}(\varphi\rho_g u_g^2) + \frac{\partial}{\partial z}((1-\varphi)\rho_l u_l u_l) + \frac{\partial P}{\partial z} = -F_{WL} - (\varphi\rho_g + (1-\varphi)\rho_l)g \tag{10}$$

Total energy balance

$$\frac{\partial}{\partial z}\left(\varphi\rho_g u_g\left(h_g + \frac{u_g^2}{2}\right)\right) + \frac{\partial}{\partial z}\left((1-\varphi)\rho_l u_l\left(h_l + \frac{u_l^2}{2}\right)\right) = \dot{q} \tag{11}$$

A real gas, Peng–Robinson equation of state was used to calculate the density of the vapour phase. The enthalpy of the vapour phase was taken as the enthalpy of the refrigerant as function of pressure and temperature, i.e., $h_g = f(P,T)$. The heat source per unit volume, $\dot{q}$, was set so as to be a known constant in the heating section and zero in the convective tube. In the above set of six governing equations there were eight unknowns, namely, the vapour phase volume fraction, φ; the mass transfer rate per volume, $\dot{m}$; the concentration, ξ, the vapour and liquid velocities, u_g and u_l, respectively; the temperature, T; and wall and vapour–liquid friction forces, F_{WL} and F_{gl}, respectively. Therefore, two additional equations for the wall and vapour–liquid friction forces were introduced to complete the model, as recommended by Richter (1983) and Yang and Zhang (2005). The wall friction, F_{WL} (Martinelli and Nelson, 1948), was given by

$$F_{WL} = \phi_{tp}^2 (dP/dz)_{F_{Lo}} \tag{12}$$

where ϕ_{tp}^2 is an empirical two-phase multiplier (Martinelli and Nelson, 1948)

$$\phi_{tp}^2 = \left(\frac{1-x}{1-\varphi}\right)^{1.75} \tag{13}$$

The pressure drop due to wall friction was calculated by

$$(dP/dz)_{F_{Lo}} = f_{Lo}(\varphi\rho_g u_g + (1-\varphi)\rho_l u_l)^2/(2(\varphi\rho_g + (1-\varphi)\rho_l)D_{pipe}) \tag{14}$$

where the friction coefficient, f_{Lo}, was calculated by (Wallis, 1969)

$$f_{Lo} = (0.79\ell nRe_{Lo} - 1.64)^{-2} \tag{15}$$

The interfacial force formulation,F_{gl}, for bubble and annular flow regimes assumed to be known. For the bubble flow regime, i.e., $\varphi < 0.3$, the interfacial force, F_{gl}, was calculated by

$$F_{gl} = \frac{3}{4}\frac{C_d^*}{d}\varphi(1-\varphi)^3\rho_l(u_g - u_l)|u_g - u_l| \tag{16}$$

The drag coefficient for a single bubble flow in liquid is well known and was calculated by

$$C_d = \begin{cases} \frac{24}{Re_d}(1 + 0.15Re_d^{0.687}) & Re_d \leqslant 1000 \\ 0.44 & Re_d > 1000 \end{cases} \tag{17}$$

The drag coefficient for the flow of many bubbles, C_d^*, takes into consideration the influence of the bubbles on each other and therefore depends on the gas phase volume fraction. Therefore, it was calculated by (Rowe and Henwood, 1961)

$$C_d^* = C_d(1-\varphi)^m \tag{18}$$

where the exponent $m = -4.7$ is almost independent of the Reynolds number (Wallis, 1969).

For the annular flow regime, i.e., $\varphi > 0.8$, the interfacial force was calculated by

$$F_{gl} = 3\frac{C_d}{D_{pipe}}\sqrt{\varphi}\rho_g(u_g - u_l)|u_g - u_l| \tag{19}$$

where the drag coefficient was calculated by (Wallis, 1969)

$$C_d = 0.005(1 + 75(1 - \varphi)) \tag{20}$$

The momentum balances of the two phases are valid for all flow regimes that might be observed in the flow boiling process, but the interfacial forces, calculated as described above, are restricted to bubble and annular flow regimes, where the gas volume fraction is below 0.3 or above 0.8, respectively. For calculating the interfacial forces in other flow regimes i.e., when the gas volume fraction is in the range of 0.3–0.8, the assumption of Richter (1983) was adopted. The drag force in the intermediate flow regimes, i.e., in plug flow, churn flow and wispy-annular flow, was linearly interpolated in between that of the bubbly and the annular drag forces with respect to the gas phase volume fraction. This assumption is rather arbitrary and can be justified only if the model predicts the flow behaviour correctly.

To calculate the drag force in the bubble flow regime, the average diameter of the bubbles must be known. This was calculated as follows. The mass transfer rate per unit volume was calculated by multiplying the number of bubbles per unit volume, N, by the mass transfer rate of a single bubble, $\dot{m}_b$, i.e., $\dot{m} = N\dot{m}_b$. The latter term was calculated by

$$\dot{m}_b = u_g\frac{d}{dx}\left(\rho_g\frac{\pi d^3}{6}\right) \tag{21}$$

and the number of bubbles per unit volume was calculated by

$$N = \frac{6\varphi}{\pi d^3} \tag{22}$$

The above sets of ordinary balance equations are complete and could therefore be solved numerically. The solution was obtained by using Gear's fifth order backward differentiation formula (BDF) method, which is available in the IMSL library. The simulation started ahead of the boiling chamber and stopped at the end of the convective tube (i.e., separation vessel).

4. Comparison between the numerical simulations and experimental data

The model was solved numerically for simulating the experiments with various heat inputs, system pressures and rich solution volumetric flow rates, for which time-averaged properties are presented in Table 2. The following inlet conditions were specified: system pressure, and solution temperature, concentration and volumetric flow rate. The inlet concentration was calculated, based on an equilibrium assumption, as a function of the reservoir temperature and the system pressure. The solution inlet velocity was calculated from the volumetric flow rate. In the transition between the single- and the two-phase models, continuous liquid properties were used, initial diameter of the bubbles was assumed to be 25 μm (Richter, 1983; Yang and Zhang, 2005), and a very small value was assumed (10^{-8} kg/m^2) for the gas mass flow rate per unit area. To conserve the total mass balance, the mass flow rate of the gas phase was subtracted from that of the liquid phase and then the gas volume fraction was calculated on the assumption that the velocities of the gas and fluid phases were similar.

By integrating the balance equations along the convective tube, we could predict the outlet conditions of the flow in the separation vessel. Since no measurements were made inside the separation vessel, two additional assumptions were made so as to validate the predictions of the numerical simulations. The first assumption was that the pressure drop across the separation vessel was negligible and therefore the predicted pressure drop was equal to the measured drop (Fig. 1). The second assumption was that the predicted volume flow rate of the poor solution was equal to the measured solution volume flow rate at the outlet of the poor solution heat exchanger. This assumption can be justified by an efficient separation process, i.e., the separated gas

Table 3
Comparison between the simulations predictions and experimental data

Heat supplied (W)	Predicted pressure drop (10^{-2} Pa)	Error $\left(\frac{\Delta P_{pr}-\Delta P_{ex}}{\Delta P_{ex}}\right)$ (%)	Experimental pressure drop SD (%)	Predicted poor solution volume flow rate (ml/min)	Error $\left(\frac{\dot{V}_{pr}-\dot{V}_{ex}}{\dot{V}_{ex}}\right)$ (%)	Experimental poor solution volume flow rate SD (%)
60	66.67	4.20	2.37	92.83	2.94	1.41
80	61.79	−1.46	2.22	96.27	0.34	4.69
100	59.00	0.56	1.95	95.20	−1.69	3.91
120	55.74	1.99	1.50	99.06	1.91	0.96
140	52.78	9.64	2.18	99.66	0.97	1.70
160	54.25	0.51	1.94	99.01	0.62	2.73
180	51.58	7.14	5.54	99.26	-0.46	1.27
200	51.35	0.27	2.97	100.47	0.99	3.75
220	50.75	0.24	5.35	95.94	1.46	2.28

would not be able to flow into the solution heat exchanger due to a liquid trap. On the basis of these assumptions, the predictions of the simulations could be compared with the experimental data.

Table 3 – presenting a comparison of the predicted poor solution volume flow rate and the pressure drop with the experimental data – clearly illustrates the validity of the model and its assumptions. The predicted mass flow rate of the poor solution deviated by less than 3% from the measured rate in all the investigated cases. The deviation of the predicted values from the average of the measured values was less than the experimental standard deviation (shown in Table 3) for most of the investigated cases. The deviations of the predicted pressure drops from the average values were up to 10%, i.e., of the same order as but larger than the experimental standard deviations (shown in Table 3). This could be explained by the sensitivity of the model to the interfacial force model [see Eqs. (16)–(20)].

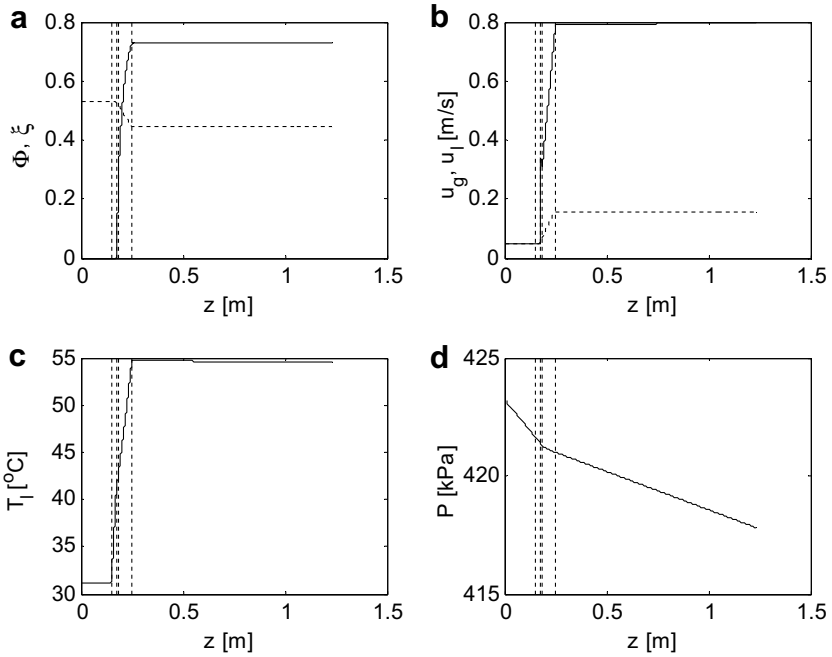

Fig. 2. Predictions of the numerical simulation of (a) gas volume fraction (solid line) and solution concentration (horizontal dashed line); (b) velocities of gas and liquid phases (solid and horizontal dashed lines, respectively); (c) temperature and (d) pressure along the vertical tube as obtained for a 160-W heat input (see Table 2). Vertical dashed lines represent locations within the heating section: the first and the last mark the location of the heating section, while the second and the third indicate the transition from sub-cooled flow to bubble flow (i.e., the transition from one- to two-phase models) and then to plug, churn or wispy-annular flow regimes.

During the experimental study, churn and wispy-annular modes of flow were observed in the convective tube. The range of the gas volume fraction that corresponds to these modes of flow is 0.6–0.8, as was predicted by the numerical simulations. Similar flow regimes were observed by Koyfman et al. (2003a,b) in an investigation of the flow boiling of an organic mixture in a bubble pump.

5. Description of the flow characteristics and parametric study

Based on the good agreement between the predictions of the model and the experimental data, it was decided to investigate the flow characteristics along the generator and the convective tube. The predictions from the numerical simulations of the gas volume fraction, solution concentration, velocities of the gas and liquid phases, temperature, and pressure along the whole vertical tube and along the heating section, for a 160-W generator are presented in Figs. 2 and 3, respectively. As can be seen in these Figures, the subcooled solution enters the vertical tube, where its pressure drops due to gravity and wall friction. It then enters the heating section, where it is heated rapidly. When the equilibrium temperature is reached (second vertical line), additional heat input results in the generation of gas (desorption of the refrigerant from the solution). The bubbles formed accelerate rapidly towards their terminal velocity. Due to the increase in the average diameter of the bubbles and the increase of gas volume fraction, the velocity of the bubbles then starts to decrease (Fig. 3b). The desorption of the refrigerant from the solution also causes a decrease in the rate of temperature change, as is to be expected, since constant heat flux is assumed and the heat transfer coefficient in flow boiling is higher than that in convective flow. When the volume fraction of the gas phase reaches 0.3, the interfacial force model is modified to account for the effects of other flow regimes. At this stage, the gas phase accelerates and drags the liquid upwards. Additional gas is then separated from the solution due to both a reduction in pressure (flashing) and an increase in temperature (heat supplied). When the two-phase flow leaves the heating section, the pressure drops continuously due to friction and gravity, resulting in minor changes in the velocities

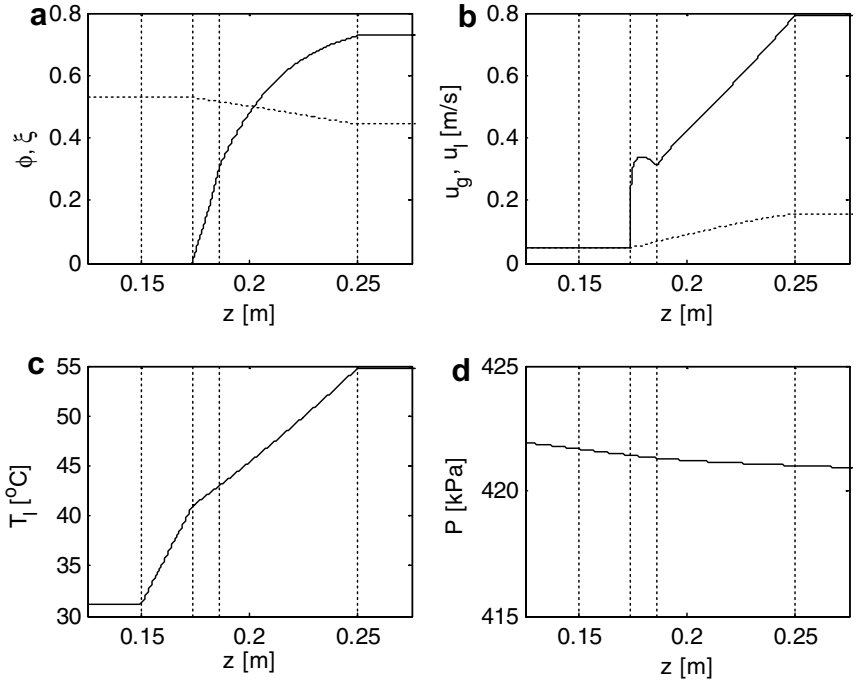

Fig. 3. Predictions of the numerical simulation of (a) gas volume fraction (solid line) and solution concentration (horizontal dashed line); (b) velocities of gas and liquid phases (solid and horizontal dashed lines, respectively); (c) temperature and (d) pressure along the heating section of the vertical tube as obtained for a 160-W heat input (see Table 2). Vertical dashed lines represent locations within the heating section: the first and the last mark the location of the heating section, while the second and the third indicate the transition from subcooled flow to bubble flow (i.e., the transition from one- to two-phase models) and then to plug, churn or wispy-annular flow regimes.

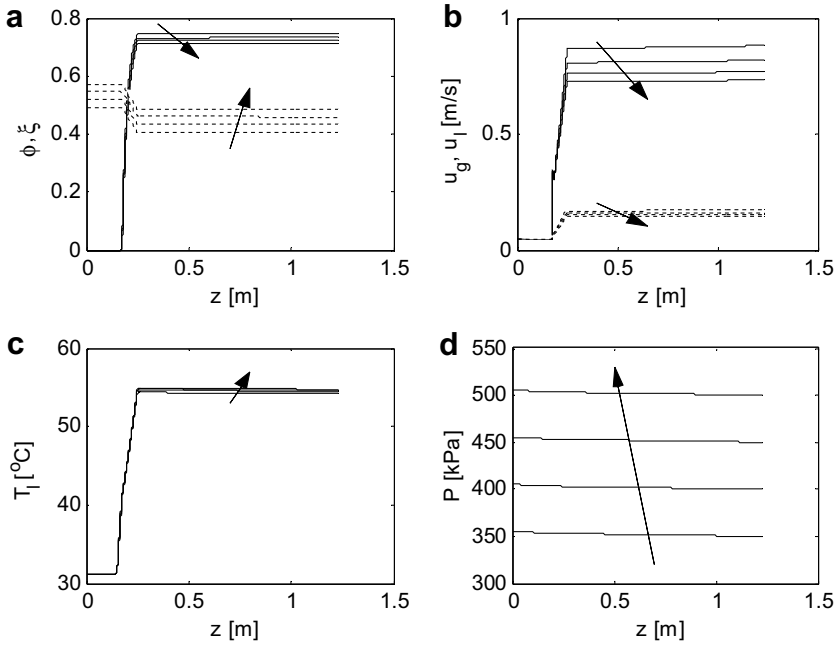

Fig. 4. Influence of the operating pressure on the predictions of the model for: (a) gas volume fraction (solid line) and solution concentration (dashed line); (b) velocities of gas and liquid phases (solid and dashed lines, respectively); (c) temperature and (d) pressure along the vertical tube as obtained for a 160-W heat input. Arrows indicate the direction of the changes in properties as a result of the increases in the operating pressure.

and temperature of the vapour and liquid phases. Since equilibrium conditions are assumed, a small reduction of the pressure causes only minor decreases in the temperature, solution concentration and gas volume fraction, which remain practically constant.

The influence of the operating pressure on the flow characteristics was examined numerically, but could not be investigated in practice since in a closed continuous system such as ours, the operating pressure and inlet temperature cannot be controlled for a given heat input. The predictions under the inlet conditions specified in Table 2 are presented in Fig. 4 for a 160-W input and four operating pressures, namely, 3.5, 4, 4.5 and 5 bars. Since the solution in the reservoir is under equilibrium conditions (see Fig. 1), it has higher refrigerant concentration at higher operating pressures (see Fig. 4a). Although more refrigerant desorbs when a solution with a higher refrigerant concentration flows through the tube (2% by weight), the gas volume fraction decreases (3.5% by volume). This resulted from the compressibility of the gas and liquid phases. The denser the gas and liquid phases, the lower their velocities (Fig. 4b). The influence of the operating pressure on the solution temperature and pressure drop was negligible (Fig. 4c and d).

The influence of the heat input at a constant operating pressure of 4 bars on the flow characteristics was examined numerically. This, too, is a theoretical case, since in a closed continuous system, such as ours, the operational pressure and inlet temperature do not remain constant as the heat input is changed. The predictions for the inlet conditions specified in Table 2 for 160-W input for four heat inputs, namely, 40, 100, 160 and 220 W, are shown in Fig. 5. As can be seen, a higher heat input results in increased desorption i.e., a reduction in refrigerant concentration at the tube exit, resulting, in turn, in a higher gas volume fraction and in increasing velocities and temperatures of the gas and liquid phases. For a lower heat input, the transition from sub-cooled single-phase flow to two-phase flow and then from bubble flow regime to other flow regimes (assumed to take place when the volume fraction of the gas phase is 0.3) occur further down stream. Fig. 5 also shows that for the 40-W heat input only the first transition occurs, i.e., the value of the gas phase volume fraction does not reach 0.3 along the vertical tube. A higher gas volume fraction results in a lower pressure drop, since the average specific volume of the fluid in the tube is much lower.

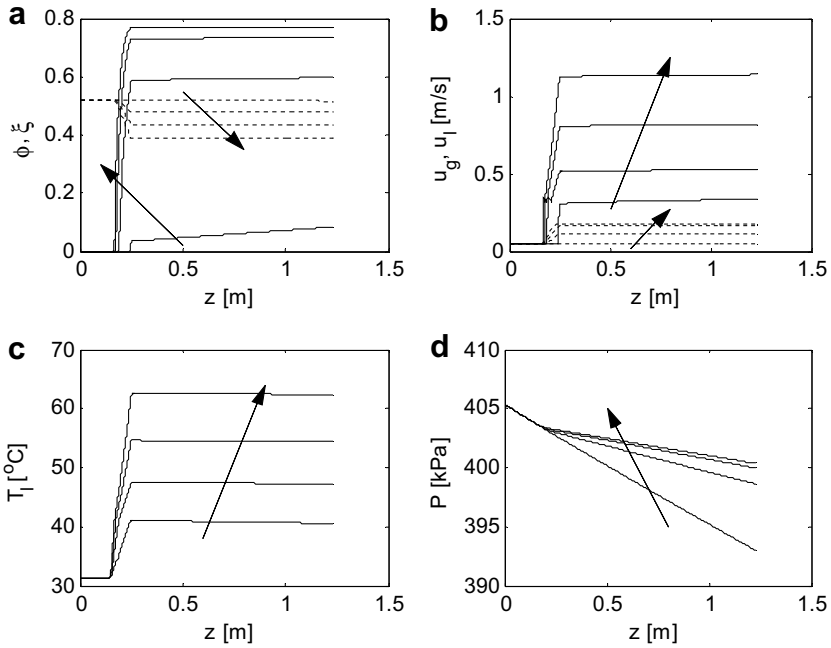

Fig. 5. Influence of the heat input on the predictions of the model for: (a) gas volume fraction (solid line) and solution concentration (dashed line); (b) velocities of gas and liquid phases (solid and dashed lines, respectively); (c) temperature and (d) pressure along the vertical tube as obtained for 40, 100, 160 and 220-W heat inputs at constant inlet conditions. Arrows indicate the direction of the change in properties a result of increasing the heat input.

6. Conclusions

A numerical and experimental study of convective boiling of a binary organic solution in a vertical tube was conducted. A continuous flow boiling experimental system was built and operated to validate the predictions of the numerical simulations. A two-fluid model was used to model and simulate the flow boiling of the binary mixture. The predictions of the numerical simulations were validated experimentally.

The assumption that due to the large difference between the normal boiling temperature of the absorbent and that of the refrigerant (more than 200 °C), the presence of absorbent vapour in the gas phase could be neglected was justified by the good agreement between the predictions of the model and the experimental data. Although the model is limited to simulating flow boiling of binary mixtures for which there is a large difference of normal boiling temperature between absorbent and refrigerant, it may be extended to simulating other binary mixtures by adding a mass balance equation for the absorbent and then calculating the gas phase properties as a function of the refrigerant concentration in the gas phase.

On the basis of the numerical simulations, a detailed description of the flow characteristics was obtained. The influence of the heat source and operating pressure on the flow characteristics was examined both numerically and experimentally.

References

Baehr, H.D., Stephan, K., 1998. Heat and Mass Transfer. Springer, Berlin.

Barbosa Jr., J.R., Hewitt, G.F., 2001a. Forced convective boiling of binary mixtures in annular flow. Part I: liquid phase mass transport. Int. J. Heat Mass Transfer 44, 1465–1474.

Barbosa Jr., J.R., Hewitt, G.F., 2001b. Forced convective boiling of binary mixtures in annular flow. Part II: heat and mass transfer. Int. J. Heat Mass Transfer 44, 1475–1484.

Bennet, D.L., Chen, J.C., 1980. Forced convective boiling in vertical tubes for saturated pure components and binary mixtures. AIChE J. 26, 454–461.

Borde, I., Jelinek, M., 1986. Thermodynamic properties of binary fluid mixtures for absorption refrigeration systems. ASME 86-WA/HT-60.

Collier, J.G., Thome, J.R., 1994. Convective Boiling and Condensation, third ed. Oxford University Press, Oxford.

Happle, O., Stephan, K., 1974. Heat transfer from nucleate to beginning of film boiling in binary mixture. In: Proceedings of the fifth International Heat Transfer Conference, Tokyo, 4, pp. 340–344.

Inoue, T., Monde, M., Teruya, Y., 2002. Pool boiling heat transfer in binary mixtures of ammonia/water. Int. J. Heat Mass Transfer 45, 4409–4415.

Jelinek, M., Levy, A., Borde, I., Density of organic binary mixtures from equilibrium measurements, Int. J. Refrig., submitted for publication.

Jung, D.S., McLinden, M., Radermacher, R., Didion, D., 1989. A study of flow boiling heat transfer with refrigerant mixtures. Int. J. Heat Mass Transfer 32, 1751–1764.

Kattan, N., Thome, J.R., Favrat, D., 1998a. Flow boiling in horizontal tubes. Part 1: development of a diabatic two-phase flow pattern map. J. Heat Transfer 120, 140–147.

Kattan, N., Thome, J.R., Favrat, D., 1998b. Flow boiling in horizontal tubes. Part 2: new heat transfer data for five refrigerants. J. Heat Transfer 120, 148–155.

Kattan, N., Thome, J.R., Favrat, D., 1998c. Flow boiling in horizontal tubes. Part 3: development of a new heat transfer model based on flow patterns. J. Heat Transfer 120, 156–165.

Koyfman, A., Jelinek, M., Levy, A., Borde, I., 2003a. An experimental investigation of bubble pump performance for diffusion absorption refrigeration system with organic working fluids. Appl. Therm. Eng. 23, 1881–1894.

Koyfman, A., Jelinek, M., Levy, A., Borde, I., 2003b. Experimental Study on Bubble Pump Performance with Organic Working Fluids. The Kielce University of Technology, Series Mechanics, pp. 25–32.

Martinelli, R.C., Nelson, D.B., 1948. Prediction of pressure drop during forced-circulation boiling of water. Trans. ASME 70, 695–702.

Mishra, M.P.H., Varma, K., Sharma, C.P., 1981. Heat transfer coefficients in forced convection evaporation of refrigerant mixtures. Lett. Heat Mass Transfer 8, 127–136.

Prashanth, K.V., Seetharamu, K.E., 1993. FEM predictions for two-phase flow in a vertical pipe without the use of any external correlations. Int. J. Numer. Meth. Heat Fluid Flows 3, 565–575.

Richter, H.J., 1983. Separated two-phase flow model: application to critical two-phase flow. Int. J. Multiphase Flow 9, 511–530.

Rivera, W., Best, R., 1999. Boiling heat transfer coefficients inside a vertical smooth tube for water\ammonia and ammonia\lithium nitrate mixtures. Int. J. Heat Mass Transfer 31, 905–921.

Ross, H.V., Radermacher, R., Di Marzo, M., Didion, D., 1987. Horizontal flow boiling of pure and mixed refrigerants. Int. J. Heat Mass Transfer 30, 979–992.

Rowe, P.N., Henwood, C.A., 1961. Drag forces in hydraulic model of a fluidized bed, part I. Trans. Inst. Chem. Eng. 39, 43–54.

Sami, S.M., Schnotale, J., Smale, J.G., 1994. Prediction of condensation and boiling characteristics of R12 substitutes R22/R152a/R114 and R22/R152a/R124 inside enhanced surface tubing. Int. J. Energy Res. 18, 727–740.

Steiner, D., Taborek, J., 1992. Flow boiling heat transfer in vertical tubes correlated by an asymptotic model. Heat transfer Eng. 13, 43–69.

Stephan, K., 1992. Heat Transfer in Condensation and Boiling. Springer-Verlag, Berlin.

Sujatha, K.S., Mani, A., Srinivasa, M.S., 1997a. Finite element analysis of a bubble absorber. Int. J. Numer. Meth. Heat Fluid Flow 7, 737–750.

Sujatha, K.S., Mani, A., Srinivasa, M.S., 1997b. Analysis of a bubble absorber working with R22 and five organic absorbents. Heat Mass Transfer 32, 255–259.

Thome, J.R., 1996. Boiling of new refrigerants: a state-of-the-art review. Int. J. Refrig. 19, 435–457.

Toral, H., Kenning, D.B.R., Shock, R.A.W, 1982. Flow boiling of ethanol/cyclohexane mixture. In: Proceedings of the Seventth international Heat Transfer Conference, Munchen, 4, pp. 255–260.

Wallis, G.B., 1969. One-dimensional Two-Phase Flow. McGraw-Hill Book Company, New York.

Wettermann, M., Steiner, D., 2000. Flow boiling heat transfer characteristics of wide-boiling mixtures. Int. J. Therm. Sci. 39, 225–235.

Wojtan, L., Thome, J.R., 2003. Flow boiling in horizontal tubes: New results for R-410a and R-134a compared to R-22. In: 21st IIR International Congress of Refrigeration, Washington DC, ICR0044.

Yang, L., Zhang, C.-L., 2005. Two-fluid model of refrigerant two-phase flow through short tube orifice. Int. J. Refrig. 28, 309–458.